

# Modulating Targeting of Poly(ethylene glycol) Particles to Tumor Cells Using Bispecific Antibodies

Jiwei Cui, Yi Ju, Zachary H. Houston, Joshua J. Glass, Nicholas L. Fletcher, Sheilajen Alcantara, Qiong Dai, Christopher B. Howard, Stephen M. Mahler, Adam K. Wheatley, Robert De Rose, Paul T. Brannon, Brett M. Paterson, Paul S. Donnelly, Kristofer J. Thurecht,\* Frank Caruso,\* and Stephen J. Kent\*

Low-fouling or “stealth” particles composed of poly(ethylene glycol) (PEG) display a striking ability to evade phagocytic cell uptake. However, functionalizing them for specific targeting is challenging. To address this challenge, stealth PEG particles prepared by a mesoporous silica templating method are functionalized with bispecific antibodies (BsAbs) to obtain PEG–BsAb particles via a one-step binding strategy for cell and tumor targeting. The dual specificity of the BsAbs—one arm binds to the PEG particles while the other targets a cell antigen (epidermal growth factor receptor, EGFR)—is exploited to modulate the number of targeting ligands per particle. Increasing the BsAb incubation concentration increases the amount of BsAb tethered to the PEG particles and enhances targeting and internalization into breast cancer cells overexpressing EGFR. The degree of BsAb functionalization does not significantly reduce the stealth properties of the PEG particles *ex vivo*, as assessed by their interactions with primary human blood granulocytes and monocytes. Although increasing the BsAb amount on PEG particles does not lead to the expected improvement in tumor accumulation *in vivo*, BsAb functionalization facilitates tumor cell uptake of PEG particles. This work highlights strategies to balance evading nonspecific clearance pathways, while improving tumor targeting and accumulation.

Dr. J. Cui, Dr. Y. Ju, Dr. Q. Dai, Prof. F. Caruso  
ARC Centre of Excellence in Convergent Bio-Nano  
Science and Technology  
and the Department of Chemical Engineering  
The University of Melbourne  
Parkville, Victoria 3010, Australia  
E-mail: fcaruso@unimelb.edu.au

Dr. J. Cui, Dr. Q. Dai  
Key Laboratory of Colloid and Interface Chemistry  
of the Ministry of Education  
School of Chemistry and Chemical Engineering  
Shandong University  
Jinan, Shandong 250100, China

Dr. Z. H. Houston, Dr. N. L. Fletcher, Dr. C. B. Howard,  
Prof. S. M. Mahler, Prof. K. J. Thurecht  
Australian Institute for Bioengineering and Nanotechnology  
The University of Queensland  
St. Lucia, Queensland 4072, Australia  
E-mail: k.thurecht@uq.edu.au

Dr. Z. H. Houston, Dr. N. L. Fletcher, Dr. C. B. Howard,  
Prof. K. J. Thurecht  
ARC Centre of Excellence in Convergent Bio-Nano Science  
and Technology  
and the Centre for Advanced Imaging  
The University of Queensland  
St. Lucia, Queensland 4072, Australia

 The ORCID identification number(s) for the author(s) of this article  
can be found under <https://doi.org/10.1002/adhm.201801607>.

Dr. J. J. Glass, S. Alcantara, Dr. A. K. Wheatley, Prof. S. J. Kent  
ARC Centre of Excellence in Convergent Bio-Nano  
Science and Technology  
and the Department of Microbiology and Immunology  
The University of Melbourne  
at the Peter Doherty Institute for Infection and Immunity  
Parkville, Victoria 3010, Australia  
E-mail: skent@unimelb.edu.au

Dr. C. B. Howard, Prof. S. M. Mahler  
ARC Training Centre for Biopharmaceutical Innovation  
The University of Queensland  
St. Lucia, Queensland 4072, Australia

Dr. R. De Rose  
ARC Centre of Excellence in Convergent Bio-Nano Science  
and Technology  
Monash Institute of Pharmaceutical Sciences  
Monash University  
381 Royal Parade, Parkville, Victoria 3052, Australia

P. T. Brannon  
Materials Characterisation and Fabrication Platform  
The University of Melbourne  
Parkville, Victoria 3010, Australia

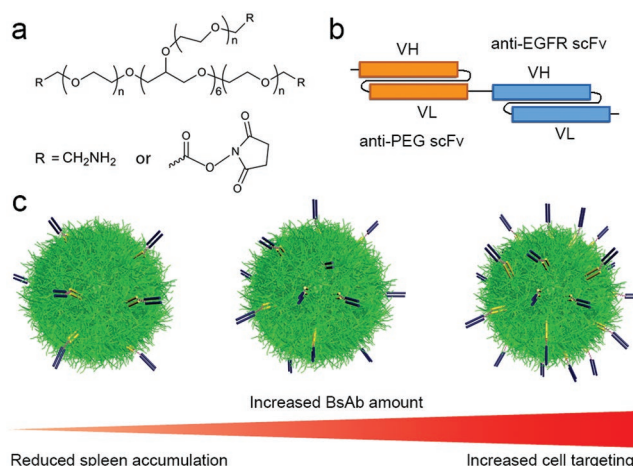
Dr. B. M. Paterson, Prof. P. S. Donnelly  
School of Chemistry and Bio21 Molecular Science  
and Biotechnology Institute  
The University of Melbourne  
Parkville, Victoria 3010, Australia

DOI: 10.1002/adhm.201801607

## 1. Introduction

The immune system provides an important defense against pathogens, but also presents a major barrier to the biomedical applications of nanoengineered particles by limiting their delivery to target cells or tissues.<sup>[1]</sup> To circumvent this barrier, a range of “stealth” materials that reduce detection and clearance of particles by the immune system have been developed.<sup>[2]</sup> The most common method used to reduce the phagocytosis of particles is surface modification with poly(ethylene glycol) (termed PEGylation).<sup>[3]</sup> The stealth properties of PEG are attributed to its ability to bind water molecules via hydrogen bonding, thus limiting its interactions with other molecules and reducing nonspecific interactions with biological systems (e.g., proteins and cells). Although PEGylation is a feasible approach to evade immune cell clearance, a high PEG density with a brush structure is typically required to maximize stealth behavior; however, regulating and simulating the PEGylation process to achieve such specific properties are challenging.<sup>[4]</sup> An alternative approach to PEGylation that we have explored is based on the engineering of stealth particles composed primarily of PEG via a mesoporous silica (MS) templating method.<sup>[5]</sup> The studies have shown that by tuning the PEG molecular weight and particle size, the *in vivo* circulation time of the PEG particles can be prolonged (>12 h) and nonspecific accumulation in the spleen and liver of mouse models is significantly decreased. Recent studies of PEG-based particles have shown their relevance for tumor therapy based on enhanced permeability and retention.<sup>[6]</sup> However, in certain biomedical applications, the delivery of particles to specific cell types is required to exert an efficient therapeutic function.<sup>[7]</sup> For example, targeted particles are required to enhance their accumulation in metastatic or blood tumors and promote cellular uptake.<sup>[8]</sup>

Among the various targeting molecules available, antibodies (Abs)—typically with two identical antigen binding domains—exhibit high selectivity and specificity for antigens, and thus have been widely used for targeted drug delivery.<sup>[9]</sup> However, the conjugation of Abs to particles typically is achieved through covalent coupling (e.g., carbodiimide chemistry, thiol-maleimide coupling, click chemistry, and periodate oxidation) between the particles and the functional groups on the antibodies. This approach typically requires multiple modification steps and can alter the affinity of the Abs to the target antigens.<sup>[10]</sup> Recently, bispecific Abs (BsAbs) have been developed with dual-epitope specificity with each arm of the Ab specific for a different epitope.<sup>[11]</sup> To target both PEG and cancer cells, BsAbs (~54 kDa) containing single-chain variable fragment (scFv) specificities, which can target both epidermal growth factor receptor (EGFR) (or ephrin type-A receptor 2, EphA2) and PEG, connected by a glycine–serine (G4S) linker, have been developed.<sup>[12]</sup> Importantly, the high stability of the BsAb conjugation has been demonstrated in our previous publications, with applications in both *in vitro* and *in vivo* models.<sup>[12]</sup> This design strategy does not rely on complex chemistry for ligation, and binding of the BsAb to both particles and target antigens can be achieved in a single step by specific chemical recognition. However, when PEG particles are modified with targeting moieties, their stealth properties



**Scheme 1.** a) Molecular structure of 8-arm-PEG. Schematic illustrations of b) a BsAb and c) the influence of BsAb amount on PEG particles on cell targeting and spleen accumulation.

may be affected by changes in the surface chemistry.<sup>[13]</sup> Therefore, it is important to investigate whether a balance that permits targeting while largely retaining an ability to evade immune system clearance can be achieved. This interplay between targeting and stealth is vital to improve drug delivery efficacy and will likely be essential to realize the full potential of targeted nanomedicines.<sup>[13,14]</sup>

Herein, we report a general strategy to engineer BsAb-functionalized PEG (PEG–BsAb) particles templated from MS templates and examine both stealth and cell targeting properties of these particles *in vitro*, *ex vivo*, and *in vivo* (**Scheme 1**). The influence of BsAb concentration, particle size, and PEG molecular weight on cell association were investigated. PEG particles (~1400 nm) with increasing amounts (from 1.6 to 9.8 fg per particle) of the anti-PEG/anti-EGFR BsAb (denoted as PEG–EGFR particles) displayed increasing targeting (from 40% to 98%, respectively) to EGFR-overexpressed breast cancer cells (MDA-MB-468), but much lower association (<10% cell association) to non-EGFR-expressed ovary cancer cells (CHO-K1) *in vitro*. When decreasing particle size, PEG–EGFR nanoparticles (~150 nm) showed high targeting to MDA-MB-468 cells (>90%) but less than 5% CHO-K1 cell association. In addition, the PEG–EGFR nanoparticles could be internalized by cancer cells after cell targeting. In the more complex environment of whole human blood, the addition of the BsAb to the PEG nanoparticle surface did not significantly increase their association with primary blood phagocytes (i.e., monocytes and granulocytes). Positron emission tomography (PET) coregistered with computed tomography (CT) was used to determine the *in vivo* biodistribution and tumor accumulation of the PEG–EGFR nanoparticles to address the balance of stealth and targeting. The PEG–EGFR nanoparticles did not show improved tumor targeting when compared with non-functionalized PEG nanoparticles; however, no significant increase in liver or spleen accumulation *in vivo* was observed when a moderate amount (<15 μg) of BsAb was used for PEG nanoparticle functionalization. Furthermore, BsAb functionalization of the PEG particles assisted cell internalization after cell targeting.

## 2. Results and Discussion

### 2.1. Preparation of PEG–BsAb Particles

PEG particles were prepared via the MS templating method.<sup>[5a]</sup> Monodisperse MS particles with average sizes of 1000 and 110 nm (denoted as MS-1000 and MS-110, respectively) were used as templates (Figure 1a,b), and 8-arm-PEG-NH<sub>2</sub> and 8-arm-PEG succinimidyl succinate (8-arm-PEG-NHS) were used as building blocks (Scheme 1a). Briefly, PEG particles were prepared by infiltration of 8-arm-PEG-NH<sub>2</sub> into the MS templates, crosslinking of 8-arm-PEG-NH<sub>2</sub> with 8-arm-PEG-NHS, followed by template removal. The PEG particles templated from MS-1000 and MS-110 are respectively denoted as PEG-1000 and PEG-110. We have previously found that PEG particles prepared using a higher molecular weight of the PEG building block, 8-arm-PEG-NHS (e.g. 40 vs 10 kDa) exhibit a lower phagocytic blood cell association.<sup>[5a]</sup> Hence, the PEG particles used herein were prepared from 40 kDa (unless specified otherwise) 8-arm-PEG-NH<sub>2</sub>. BsAbs comprising anti-PEG scFv and anti-EGFR scFv (Scheme 1b) were used to functionalize the PEG particles for the cell targeting studies. As a negative control, anti-PEG/anti-EphA2 BsAb-functionalized PEG particles (denoted as PEG–EphA2 particles) were also prepared. Following exposure of 10<sup>9</sup> PEG-1000 particles to BsAb solution (40 μg in 150 μL), the zeta-potential of the PEG-1000 particles altered from ≈0 to –10 mV, indicating the presence of BsAbs on the PEG-1000 particles. To image the PEG-1000 and PEG-110 particles, Alexa Fluor 633 carboxylic acid succinimidyl ester (AF633) was used to fluorescently label the amine groups in the PEG particles during the particle preparation step. As shown in

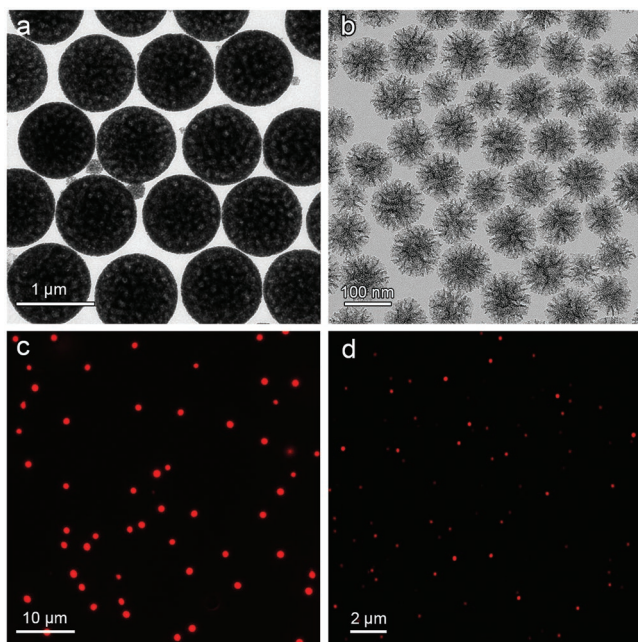


**Figure 1.** TEM images of a) MS-1000 and b) MS-110 template particles. Fluorescence images of AF633-labeled c) PEG-1000-EGFR and d) PEG-110-EGFR particles prepared using MS-1000 and MS-110 templates, respectively. The PEG particles were prepared from 40 kDa 8-arm-PEG-NH<sub>2</sub>.

the fluorescence microscopy images (Figure 1c,d), PEG-1000-EGFR (1400 ± 100 nm) and PEG-110-EGFR (150 ± 30 nm) particles are well dispersed and exist as individual particles in aqueous solution. The size of the PEG-110 particles before and after BsAb functionalization was similar (150 ± 30 nm) based on structured illumination microscopy (SIM) analysis (data not shown).

### 2.2. Cancer Cell Targeting and Internalization of PEG–BsAb Particles

To assess the cell surface expression of EGFR and EphA2, phycoerythrin (PE)-labeled anti-EGFR or anti-EphA2 was incubated with MDA-MB-468, MDA-MB-231, and CHO-K1 cells. Flow cytometry confirmed that MDA-MB-468 cells highly expressed EGFR compared to EphA2, and MDA-MB-231 cells expressed both EGFR and EphA2 on their surfaces, whereas the CHO-K1 cells did not express any of the antigens studied (Figure S1, Supporting Information). Previous work has reported that antilipopolysaccharide/anti-EGFR BsAb-modified EDV nanocells can target MDA-MB-468 cells.<sup>[15]</sup> Therefore, MDA-MB-468 cells were chosen as target cells for the in vitro and in vivo studies. To investigate the influence of BsAb concentration on cell targeting, PEG-1000 particles were incubated with different amounts of BsAbs in 150 μL Dulbecco phosphate-buffered saline (DPBS) at 4 °C for 15 h, followed by incubation with MDA-MB-468 cells for 24 h. The amount of BsAb per PEG particle varied from 1.6 to 9.8 fg (corresponding to a BsAb number per particle range from 1.7 × 10<sup>4</sup> to 1.1 × 10<sup>5</sup>) when 5, 10, 20, or 40 μg of BsAb was incubated with 10<sup>9</sup> PEG-1000 particles (163 μg) (Figure S2, Supporting Information). Confocal laser scanning microscopy (CLSM) demonstrated the presence of BsAbs within and on the surface of the PEG particles (Figure S3, Supporting Information).

PEG-1000-EGFR particle targeting to MDA-MB-468 cells increased considerably as a function of the amount of BsAb per particle, with around 40%, 75%, 92%, and 98% cell targeting observed when 1.6, 3.2, 5.8, and 9.8 fg of BsAb were functionalized on individual PEG-1000 particles, respectively (Figure 2a). Though the percentage of cell association was above 90% when 20 or 40 μg of BsAb was used for particle functionalization, the mean fluorescence intensity (MFI) of cells that were incubated with PEG-1000-EGFR particles functionalized with 9.8 fg of BsAb was 2.7 times higher than the MFI of the cells that were incubated with PEG-1000-EGFR particles functionalized with 5.8 fg (Figure 2b). This suggests that the presence of a larger amount of BsAb per PEG particle results in increased cell targeting. Therefore, 9.8 fg of BsAb per PEG particle was chosen for subsequent cell targeting studies. As previously reported by us, increasing the PEG molecular weight (from 10 to 40 kDa) reduces phagocytic blood cell association of the PEG particles.<sup>[5a]</sup> To investigate the influence of PEG molecular weight on cell targeting, 10 or 40 kDa 8-arm-PEG-NH<sub>2</sub> was used to fabricate PEG particles for BsAb functionalization. As shown in Figure 2c, negligible (<1%) nonspecific association of PEG-1000 particles was observed. Though PEG-1000-EGFR particles assembled with 10 kDa PEG resulted in higher (96%) cell targeting compared with PEG-1000-EGFR particles assembled

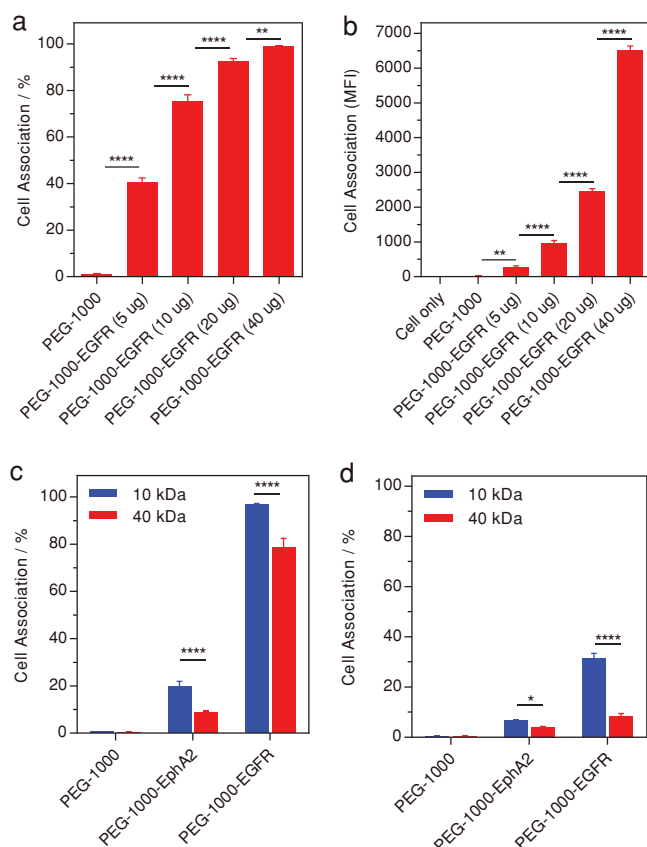


**Figure 2.** a,b) Influence of the amount of anti-PEG/anti-EGFR BsAb (1.6, 3.2, 5.8, and 9.8 fg) per PEG-1000 particle on cell association with MDA-MB-468 cells (cell-to-particle ratio 1:50). The PEG particles were prepared from 40 kDa 8-arm-PEG-NH<sub>2</sub>. c,d) Influence of 8-arm-PEG-NH<sub>2</sub> molecular weight used for PEG particle assembly on (c) MDA-MB-468 and (d) CHO-K1 cell association. BsAbs (40 µg) were incubated with 10<sup>9</sup> PEG-1000 particles (163 µg) in 150 µL DPBS at 4 °C for 15 h, resulting in 9.8 fg of BsAb per particle, before incubation with cells at a cell-to-particle ratio 1 to 50 (equivalent to 8.15 pg of particles per cell) at 37 °C for 24 h. Cell association measured as a percentage or mean fluorescence intensity (MFI) was determined by flow cytometry. Data represent means ± standard deviations based on triplicate experiments (one-way ANOVA using Tukey's multiple comparisons test for (a,b) and two-way ANOVA using Tukey's multiple comparisons test for (c,d), \**p* < 0.05, \*\**p* < 0.01, \*\*\*\**p* < 0.0001).

with 40 kDa PEG (78%), nonspecific association of PEG-1000-EphA2 particles assembled with 10 kDa PEG was two times higher than that of PEG-1000-EphA2 particles assembled with 40 kDa PEG (9%). The high targeting specificity of PEG-1000-EGFR particles was also confirmed by CLSM (Figure S4, Supporting Information). Almost no cell association was observed for the PEG-1000 particles and 10% of cells were observed to associate with PEG-1000-EphA2 particles. By contrast, around 80% of the MDA-MB-468 cells could be targeted by the PEG-1000-EGFR particles, which is consistent with the flow cytometry results (Figure 2c). As CHO-K1 cells do not express either EGFR or EphA2 antigens, nonspecific CHO-K1 cell interactions with both PEG-1000-EphA2 and PEG-1000-EGFR particles were investigated (Figure 2d). PEG-1000-EphA2 and PEG-1000-EGFR particles assembled with 40 kDa PEG

showed less than 5% and 10% CHO-K1 cell association, respectively, whereas the PEG-BsAb particles assembled with 10 kDa exhibited 2–3 times higher cell association. This result indicates that the PEG-BsAb particles assembled with 40 kDa 8-arm-PEG-NH<sub>2</sub> retain their stealth properties to non-EphA2- or non-EGFR-expressed cancer cells. Therefore, 40 kDa PEG was used to fabricate smaller PEG particles for the investigation of stealth and targeting.

According to the optimized in vitro experiments based on PEG-1000-BsAb particles, 163 µg of PEG-110 particles were incubated with 40 µg of BsAb for particle functionalization, followed by cell association studies with MDA-MB-468 and CHO-K1 cells. As shown in Figure 3, PEG-110-EGFR particles had high targeting specificity (>90%) to MDA-MB-468 cells.

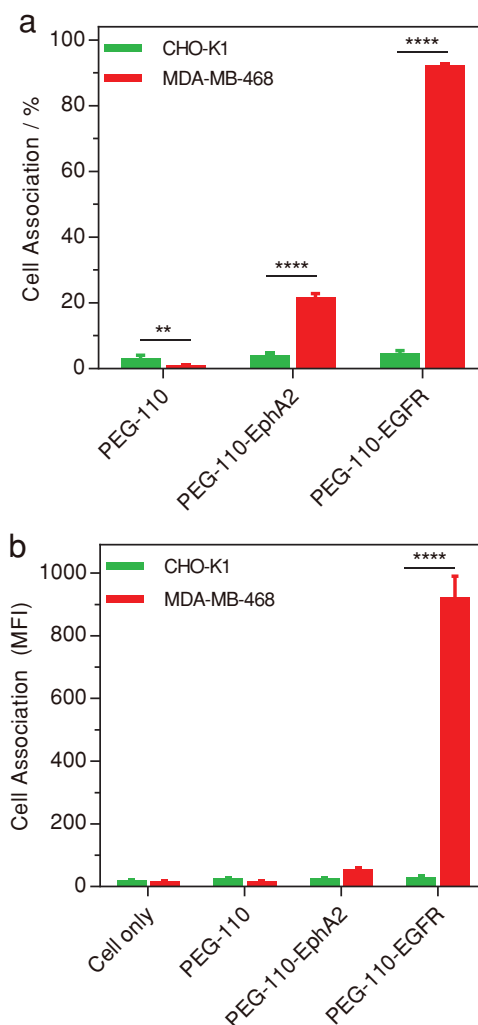


**Figure 3.** MDA-MB-468 and CHO-K1 cell association of PEG-110, PEG-110-EphA2, and PEG-110-EGFR particles assembled with 40 kDa 8-arm-PEG. Cell association with particles was determined by flow cytometry and represented as a) percentage of cell association or b) MFI. BsAbs (40 µg) were incubated with 163 µg of PEG-110 particles in 150 µL DPBS at 4 °C for 15 h before incubation with cells (8.15 pg of particles per cell) at 37 °C for 24 h. Data represent means ± standard deviations based on triplicate experiments (two-way ANOVA using Tukey's multiple comparisons test, \*\**p* < 0.01, \*\*\*\**p* < 0.0001).

Though PEG-110-EphA2 particles showed about 20% cell association with MDA-MB-468 cells, the MFI of these cells is much lower compared with that of the cells that were incubated with PEG-110-EGFR particles. Importantly, both PEG-110-EGFR and PEG-110-EphA2 particles were stealthy to CHO-K1 cells, similar to PEG-110 particles.

For drug delivery applications, efficient internalization of the drug carriers is critical to delivering drugs into cancer cells.<sup>[16]</sup> It is known that some Abs assist only in the targeting of particles to cancer cell surfaces but do not promote specific receptor-mediated internalization.<sup>[17]</sup> By contrast, functionalizing nanoparticles with anti-EGFR Ab can efficiently target cancer cells while also mediating cell internalization.<sup>[18]</sup> To investigate the internalization of PEG-110-EGFR particles into cells, the particles were labeled with AF488 for super-resolution imaging by SIM. Both CLSM and SIM images indicate a high targeting specificity of PEG-110-EGFR particles and stealth properties of PEG and PEG-110-EphA2 particles to MDA-MB-468 cells (Figure 4; Figure S5, Supporting Information), which is consistent with the flow cytometry results. In addition, multiple

PEG-110-EGFR particles labeled with AF488 (green dots) were identified inside the MDA-MB-468 cell membrane, indicating the internalization of the PEG-110-EGFR particles (Figure 4).

### 2.3. Balancing Targeting and Stealth Properties

Although surface modification of PEG-1000 and PEG-110 particles with BsAbs can improve cell targeting, one important question is whether the presence of BsAbs can increase phagocytic clearance following intravenous administration? To examine their stealth properties in a complex immune cell environment, we used a previously described ex vivo human blood assay that has a higher sensitivity than a cell line assay and examined particle association by primary phagocytes (i.e., monocytes and granulocytes) in their natural milieu (Figure 5a; Figure S6, Supporting Information).<sup>[5a,c]</sup> As shown in Figure 5b, both monocyte and granulocyte association of PEG-1000-BsAb particles increased as a function of the amount of BsAb used for particle functionalization regardless of the type of BsAb. These

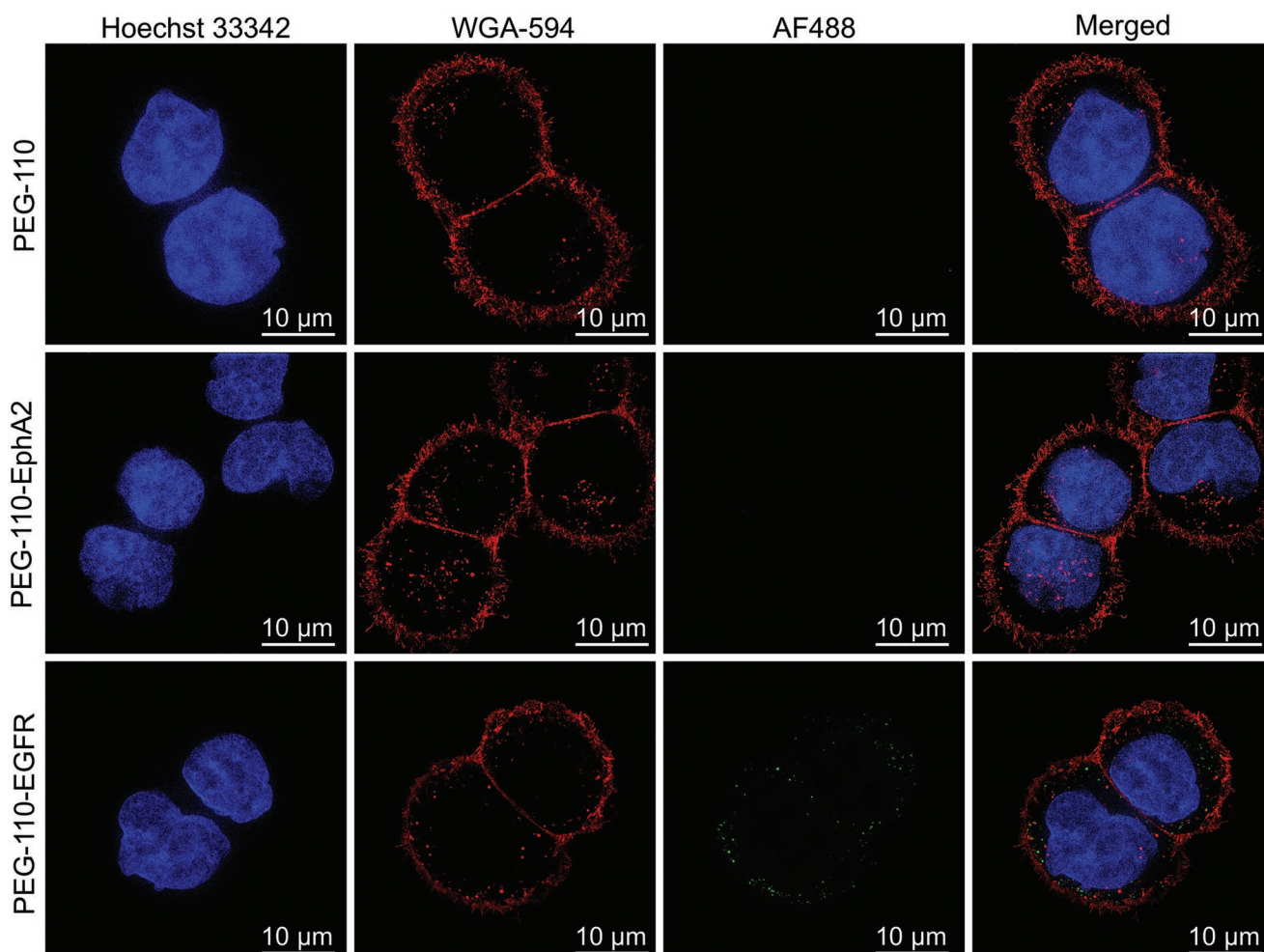


**Figure 4.** Super-resolution microscopy images of MDA-MB-468 cells incubated with PEG-110, PEG-110-EphA2, and PEG-110-EGFR particles. BsAbs (40  $\mu$ g) were incubated with 163  $\mu$ g PEG-110 particles in 150  $\mu$ L DPBS at 4  $^{\circ}$ C for 15 h before incubation with cells. Cell nuclei and membranes were stained with Hoechst 33 342 (blue) and WGA-AF594 (red), respectively. Particles were fluorescently labeled with AF488 (green). Cells were incubated with the particles (8.15 pg of particles per cell) at 37  $^{\circ}$ C for 24 h.

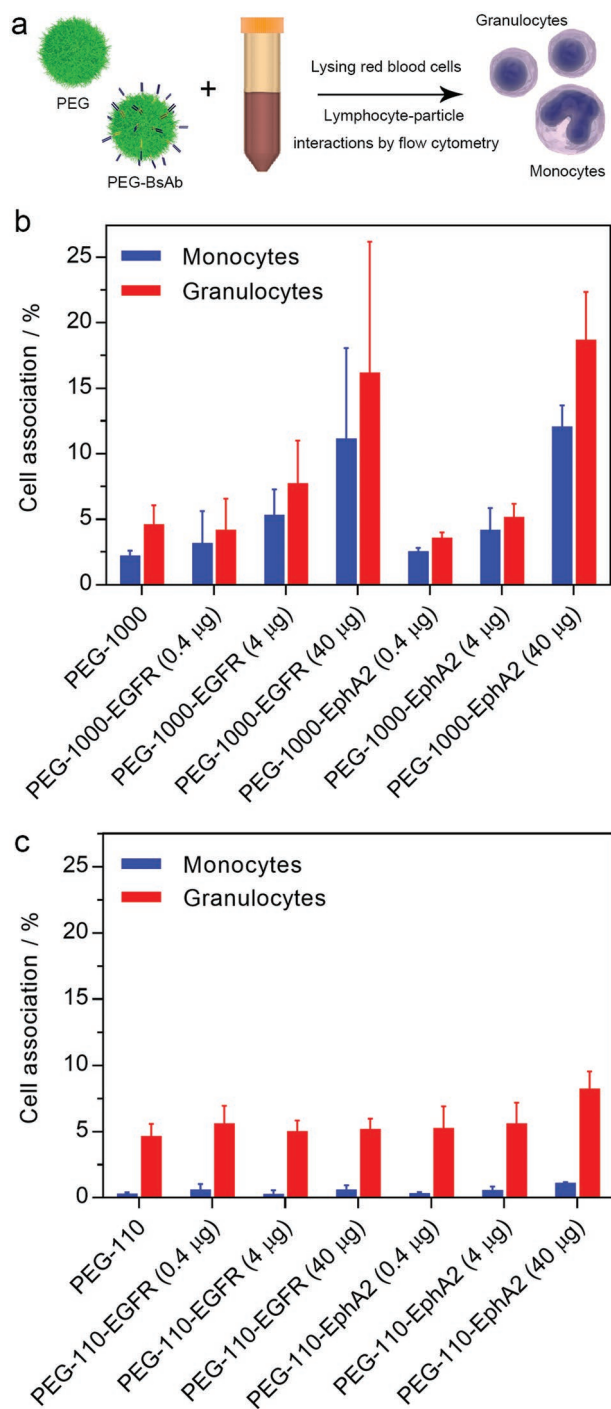


**Figure 5.** a) Schematic illustration of ex vivo human blood assay to investigate particle association with primary phagocytes. b,c) Monocyte and granulocyte association of PEG-1000, PEG-1000-EGFR, PEG-1000-EphA2 particles (b), and PEG-110, PEG-110-EGFR, and PEG-110-EphA2 particles (c). PEG-1000 or PEG-110 particles (163 μg) were incubated with 0.4, 4, or 40 μg of anti-PEG/anti-EGFR BsAb or anti-PEG/anti-EphA2 BsAb in 150 μL DPBS at 4 °C for 15 h. The particles were then incubated with freshly drawn whole human blood (8.15 pg of particles per cell) at 37 °C for 1 h. Red blood cells were lysed and cells phenotyped using a fluorescent antibody cocktail. Cell association with the particles was examined by flow cytometry. Data represent means ± standard deviations based on triplicate experiments.

cell association values were lower than 20% even when 40 μg of BsAb was used for PEG particle functionalization. In addition, cell association did not show any significant changes before or after functionalization of BsAbs on PEG-110 particles (Figure 5c). These results indicate that BsAb modification does not influence the stealth properties of PEG-110-BsAb particles ex vivo.

#### 2.4. Biodistribution and Tumor Accumulation

The biological behaviors of the PEG-BsAb particles were further investigated in vivo to explore the balance of their stealth and targeting properties. PEG-110 particles were used for the in vivo studies, as our previous studies<sup>[5a]</sup> showed that smaller PEG particles have longer circulation times than larger PEG particles. For the quantification of BsAb per particle, MS@PEG-110 particles (template present) were incubated with different amounts (i.e., 5, 10, 15, and 20 μg) of anti-PEG/anti-EGFR BsAbs. MS@PEG-110 particles were employed for quantification because keeping the core enables particles to be easily separated by centrifugation after incubation with BsAbs. We assume that the amount of BsAb per MS@PEG-110 particle is similar to the amount of BsAb per PEG-110 particle. The amount of BsAb per MS@PEG-110 particle varied from 0.004 to 0.015 fg (the number of BsAbs per PEG particle varied from 45 to 173) (Figure S7, Supporting Information). This indicates that a larger amount of BsAb per PEG particle is obtained when a larger amount of BsAb is used for incubation. For in vivo studies, PEG-110 particles were labeled with <sup>64</sup>Cu via a macrobicyclic cage amine ligand sarcophagine (MeCOSar-NHS), as described previously,<sup>[5a]</sup> and functionalized with BsAbs before intravenous injection. The biodistribution of PEG-110 and PEG-110-EGFR particles was qualitatively examined by PET-CT imaging of tumor-bearing mice. As shown in **Figure 6**, there is little difference between the accumulation of PEG-110 particles in the EGFR-overexpressed tumors when compared with that observed for PEG-110-EGFR particles at the time points measured. However, the accumulation of PEG-110-EGFR particles in the spleen was ≈1.5-fold higher than that of the PEG-110 particles ( $p < 0.001$ ). This may be attributed to BsAb functionalization influencing the stealth properties of PEG-110 particles in the more complex in vivo environment.

To further quantitatively investigate the influence of BsAb concentration on the biodistribution of PEG-110-EGFR particles, PEG-110 particles were incubated with 5, 15, and 20 μg of anti-PEG/anti-EGFR BsAbs (corresponding to 45, 149, and 173 of BsAbs per MS@PEG-110 particle under the same conditions, Figure S7, Supporting Information) and injected into mice. At 48 h postinjection, organs were dissected and subjected to gamma counting to quantify biodistribution of the PEG-110-EGFR particles. The values for each organ were averaged across the set of mice ( $n = 3$ ) and the standard deviation was used as the error to generate the biodistribution plots (**Figure 7**). The biodistribution of PEG-110-EGFR particles in different organs, except for spleen, was comparable. In general, tumor accumulation was slightly higher when a lower anti-PEG/anti-EGFR BsAb concentration was used. However, spleen accumulation of PEG-110-EGFR incubated with 20 μg of BsAb

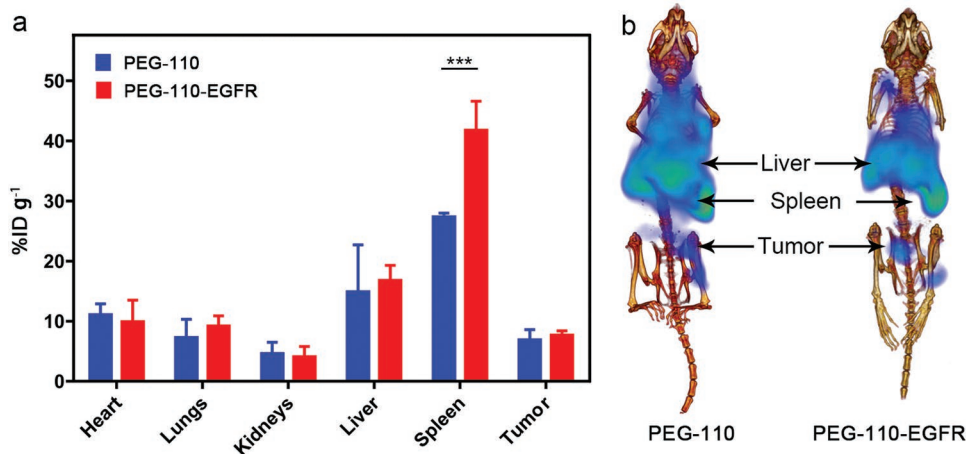


**Figure 6.** a) In vivo biodistribution and tumor accumulation of both PEG-110 and PEG-110-EGFR particles at 24 h postinjection of <sup>64</sup>Cu-labeled PEG-110 and <sup>64</sup>Cu-labeled PEG-110-EGFR particles in mice bearing subcutaneous MDA-MB-468 tumors, highlighting increased spleen uptake as a result of the BsAb modification; the data are reported as percentage of injected dose per gram of tissue (%ID g<sup>-1</sup>). Data represent means ± standard deviations based on triplicate experiments (two-way ANOVA using Tukey's multiple comparisons test, \*\*\**p* < 0.001). b) Representative PET-CT images at 48 h postinjection of <sup>64</sup>Cu-labeled PEG-110 and <sup>64</sup>Cu-labeled PEG-110-EGFR particles with highlights for liver, spleen, and tumor uptake. PEG-110-EGFR particles were obtained by incubating BsAbs (20 μg) with PEG-110 particles (templated from 2 mg of MS-110, 2.6 × 10<sup>12</sup> particles).

was significantly higher than that of PEG-110-EGFR particles when lower concentrations of BsAbs were used. As indicated by the amount of BsAb per MS@PEG-110 particles (Figure S7, Supporting Information), incubation with more BsAbs likely results in larger amounts of BsAbs per PEG particle. It is also likely that the increased spleen accumulation is due to the large amount of BsAb on PEG-110 particles influencing their stealth properties. Therefore, in this particular study, 15 μg of BsAb could be used to minimize off-target accumulation. However, this value will vary depending on the particles used and the targeting ligand chosen.

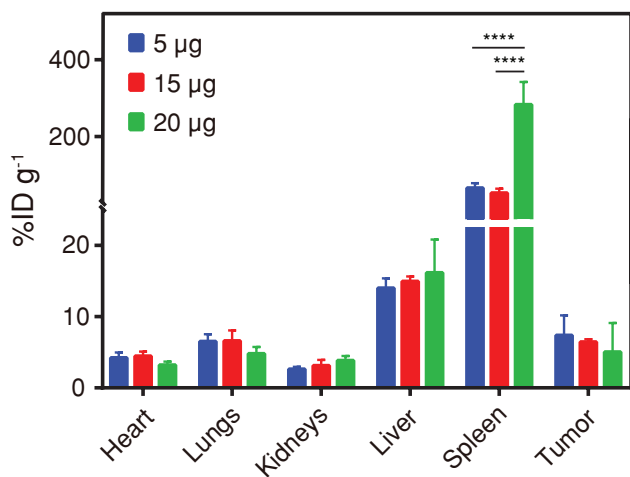


**Figure 7.** Ex vivo biodistribution and tumor accumulation of <sup>64</sup>Cu-labeled PEG-110-EGFR particles in mice bearing subcutaneous MDA-MB-468 tumors at 48 h postinjection; the data are reported as %ID g<sup>-1</sup>. Data represent means ± standard deviations based on triplicate experiments (two-way ANOVA using Tukey's multiple comparisons test, \*\*\*\**p* < 0.0001). The particles were templated from MS-110 and functionalized with varying amounts (5, 15, and 20 μg) of BsAb.

### 3. Conclusion

We have demonstrated the assembly of PEG–BsAb particles and studied their biological behavior in vitro, ex vivo, and in vivo. PEG–EGFR particles displayed higher cancer cell targeting in vitro when higher concentrations of BsAbs were used to functionalize the PEG particles. The PEG–EGFR particles assembled from larger molecular weight PEG (40 kDa) and/or smaller MS templates (≈110 nm) displayed high association with EGFR overexpressing cancer cell line (MDA-MB-468) while retaining low nonspecific association with the EGFR minimal-expressing cell line (CHO-K1). In addition, the PEG–EGFR particles could induce tumor cell uptake following cell targeting in vitro, which is favorable for intracellular drug delivery. BsAb functionalization on PEG particles (≈150 nm) does not significantly influence their association with monocytes and granulocytes ex vivo. Though BsAb functionalization did not significantly improve tumor targeting in mice, no significant increase in liver or spleen accumulation in vivo was observed when a moderate amount of BsAb was used for PEG particle functionalization. This work shows that BsAb-functionalized PEG particles can exhibit different biological behaviors. The trade-off between stealth properties and cell targeting following BsAb functionalization of PEG particles yields different results in vitro and in vivo. Given the complexity of in vivo conditions, in vitro and ex vivo studies may provide directional but limited insight into the use of targeted stealth particles. Further studies are warranted to investigate and model the optimal balance of targeting and stealth properties in vivo as well as for drug delivery applications.

### 4. Experimental Section

**BsAb Synthesis:** The BsAbs generated comprised two scFvs joined by a G4S linker. One scFv sequence was specific for PEG,<sup>[19]</sup> with the

second scFv sequence specific for a cancer cell surface receptor (EGFR<sup>[20]</sup> or EphA2<sup>[21]</sup>). BsAbs were expressed in Chinese hamster ovary CHO-S cells as previously described.<sup>[12]</sup> Briefly, genes encoding the BsAbs were synthesized by GeneArt (Invitrogen). A 6× His motif (for affinity purification) and a c-Myc epitope (for detection by fluorescent anti-Myc Abs) were included at the N- and C-termini, respectively. The BsAb genes were cloned into a mammalian expression plasmid (pcDNA 3.1 (+), Invitrogen) using HindIII and NotI restriction sites. Plasmid DNA (2 μg mL<sup>-1</sup>) was complexed with polyethylenimine (PEI)-Pro (PolyPlus) in Opti-Pro serum free medium (Life Technologies) at a DNA (μg) to PEI (μL) ratio of 1:4 (w/v) for 15 min before transiently transfecting suspension-adapted CHO-S cells (3 × 10<sup>6</sup> mL<sup>-1</sup>). Cells were grown in chemically defined CHO medium (CD-CHO, Life Technologies) at 37 °C, 7.5% CO<sub>2</sub> with shaking (130 rpm) for 6 h, before adding 7.5% CD-CHO Efficient Feed A (Life Technologies), 7.5% CD-CHO Efficient Feed B (Life Technologies), and 0.4% anticlumping agent (Gibco), and culturing at 32 °C, 7.5% CO<sub>2</sub> with shaking for 7–14 days. Cells were cultured until their viability reduced below 50% as measured by trypan blue exclusion. Following expression, BsAbs were purified by pelleting cells by centrifugation (5250 g, 30 min), filtering supernatant through a 0.22 μm membrane (Sartorius), and purifying with a 5 mL HisTrap excel column (GE Healthcare). BsAbs were eluted with 20 × 10<sup>-3</sup> M sodium phosphate, 500 × 10<sup>-3</sup> M sodium chloride, and 500 × 10<sup>-3</sup> M imidazole at pH 7.4. Alternatively, a 5 mL Protein L column was used, with BsAbs eluted using 100 × 10<sup>-3</sup> M glycine at pH 3.0. Following buffer exchange and size exclusion chromatography, the BsAbs were filtered through 0.22 μm membranes and stored at 0.25–0.60 mg mL<sup>-1</sup> in buffer containing 20 × 10<sup>-3</sup> M sodium phosphate and 500 × 10<sup>-3</sup> M sodium chloride at pH 7.6. The BsAbs (0.5 mg mL<sup>-1</sup>, 1000 μL in DPBS) were buffer-exchanged into 0.1 M Na<sub>2</sub>CO<sub>3</sub> buffer and labeled with AF488 NHS ester (1 mg mL<sup>-1</sup>, 24 μL in dimethyl sulfoxide (DMSO)) or Cyanine 5 NHS ester (1 mg mL<sup>-1</sup>, 22 μL in DMSO) in DPBS for 4 h at 4 °C. The solution was then purified by preparative size exclusion chromatography in DPBS, collecting the first eluting peak. The combined fractions were reduced in volume using Amicon spin filters (3000 molecular weight cutoff (MWCO)) to achieve a final concentration of 0.5 mg mL<sup>-1</sup>.

**Fabrication of PEG and PEG–BsAb Particles:** MS-1000 particles were synthesized using polyelectrolyte–surfactant complexes as templates.<sup>[5a,22]</sup> MS-110 particles were synthesized by a previously reported method.<sup>[23]</sup> PEG particles were prepared based on an MS templating method according to a previous protocol.<sup>[5a,24]</sup> For fluorescence imaging, PEG-1000 and PEG-110 particles were labeled with AF633 or AF488. For PET studies, MeCOSar-NHS were synthesized and functionalized on PEG-110 particles for coordinating positron-emitting <sup>64</sup>Cu.<sup>[5a]</sup> To quantify the weight of PEG particles, the PEG-1000 and PEG-110 particle suspensions (synthesized from 54 mg MS-1000 and MS-110, respectively) in water were freeze-dried and weighed. To functionalize PEG-1000 particles with BsAbs, 10<sup>9</sup> particles (equivalent to 163 μg) in DPBS (150 μL) were incubated with BsAbs (0.4 to 40 μg) at 4 °C for 15 h, followed by washing twice with DPBS (9000 g, 10 min). To functionalize PEG-110 particles with BsAbs, the particles (163 μg) in DPBS (150 μL) were incubated with BsAbs (0.4, 4, or 40 μg) at 4 °C for 15 h. The binding constant for anti-PEG/anti-EGFR bispecific antibodies reported in this paper has been reported to have nM affinity ( $K_D$  of 10 × 10<sup>-9</sup> M) and this is consistent with reported affinities for whole IgG1 immunoglobulins against PEG, which have a  $K_D$  of 1.9 × 10<sup>-9</sup> M to 3.0 × 10<sup>-9</sup> M against linear PEG chains.<sup>[25]</sup>

**Quantification of Anti-PEG/Anti-EGFR BsAb per PEG-1000 and MS@PEG-110 Particles:** PEG-1000 particles (163 μg) or MS@PEG-110 particles (163 μg) were incubated with cyanine 5-labeled anti-PEG/anti-EGFR BsAbs (5 to 40 μg) in DPBS (150 μL) at 4 °C for 15 h. The PEG-1000 and MS@PEG-110 particles were centrifuged (12 000 g for 15 min) and the fluorescence intensity of the supernatant was measured. The amount and number of BsAbs per PEG-1000 and MS@PEG-110 particle were quantified from a fluorescence curve of cyanine 5-labeled anti-PEG/anti-EGFR BsAb.

**Cell Culture:** MDA-MB-468 (American Type Culture Collection (ATCC)) and CHO-K1 (ATCC) cells were cultured in RPMI 1640 medium (Life

Technologies), supplemented with 10% fetal bovine serum (FBS) (Life Technologies), and 1% L-glutamine (Sigma-Aldrich) at 37 °C in 5% CO<sub>2</sub>. MDA-MB-231 cells (ATCC) were cultured in Dulbecco's modified Eagle medium (Thermo Fisher Scientific), supplemented with 10% FBS (Life Technologies) at 37 °C in 5% CO<sub>2</sub>. MDA-MB-468, CHO-K1, and MDA-MB-231 cells with passage number 10–30 were used in the study and all cells passed the mycoplasma test.

**EGFR Expression Study:** Cell surface expression of EGFR was determined by detaching MDA-MB-468, MDA-MB-231, or CHO-K1 cells using trypsin. The detached cells (10<sup>6</sup> cells) were then incubated with anti-EGFR-PE or anti-EphA2-PE (0.5 μg, BioLegend) in 3% bovine serum albumin (BSA) in DPBS for 30 min on ice. After washing the cells with DPBS, at least 2 × 10<sup>4</sup> cells were analyzed by flow cytometry for PE fluorescence (Apogee A50-Micro flow cytometer).

**Cell Association Analysis by Flow Cytometry:** MDA-MB-468 and CHO-K1 cells were seeded in 24-well plates with 70 000 cells per well and allowed to adhere overnight. AF633-labeled PEG-1000, PEG-1000-EphA2, PEG-1000-EGFR, PEG-110, PEG-110-EphA2, or PEG-110-EGFR particles were added into cell media at a ratio of 8.15 pg of particles per cell and incubated with the cells for 24 h (37 °C, 5% CO<sub>2</sub>). After incubation, the cells were washed three times with DPBS and collected by trypsinization, followed by centrifugation at 400 g for 5 min. The cell pellet was resuspended in DPBS and analyzed using flow cytometry (Apogee A50-Micro flow cytometer).

**Cell Imaging by CLSM and SIM:** MDA-MB-468 cells were seeded at a density of 40 000 cells per well in an 8-well Lab-Tek chambered coverglass slides (Thermo Fisher Scientific) and allowed to adhere overnight. Cells were then incubated with the PEG-1000, PEG-1000-EphA2, PEG-1000-EGFR, PEG-110, PEG-110-EphA2, or PEG-110-EGFR particles at a particle-to-cell ratio of 8.15 pg of particles per cell for 24 h (37 °C, 5% CO<sub>2</sub>), followed by three washes with DPBS. Cells were fixed with 4% paraformaldehyde in DPBS (200 μL) at 25 °C for 15 min, followed by three washes with DPBS. The fixed cells were stained with Wheat germ agglutinin AF488 conjugate (WGA-AF488) or WGA-AF594 (5 μg mL<sup>-1</sup> in DPBS) on ice for 10 min and Hoechst 33 342 (5 μg mL<sup>-1</sup> in DPBS) for 15 min and washed with DPBS twice. Fluorescence microscopy images of cells were obtained on a Nikon A1R confocal microscope with a 60× oil immersion objective with standard DAPI/FITC/TRITC/CY5 filter sets. Super-resolution images were acquired on a DeltaVision OMX structure illumination microscope (Applied Precision) operating in SIM mode to obtain an approximate resolution of 110 nm in X/Y and 250 nm in Z.

**Blood Cell Association:** Fresh whole blood (FWB) was collected from healthy human donors after obtaining informed consent in accordance with The University of Melbourne Human Research Ethics approval (No. 1443420) and the Australian National Health and Medical Research Council Statement on Ethical Conduct in Human Research. Blood was drawn by venepuncture into Vacuette collection tubes containing sodium heparin (Greiner Bio-One) and gently inverted five times.

Freshly drawn blood (100 μL) was introduced into FACS tubes and incubated at 37 °C for 10 min. PEG-1000, PEG-1000-EphA2, PEG-1000-EGFR, PEG-110, PEG-110-EphA2, or PEG-110-EGFR particles were added directly to whole blood at a particle-to-white blood cell (WBC) ratio of 8.15 pg particle per cell (4 μg particles per 100 μL blood containing ≈5 × 10<sup>5</sup> cells) and incubated for 1 h at 37 °C, before placing all tubes on ice. Erythrocytes were lysed with Pharm Lyse buffer (2 mL, BD Biosciences) and topped up to 4 mL using 1 × PBS. WBCs were pelleted (500 g, 5 min) and washed twice with PBS. Cells were phenotyped on ice (1 h) using optimized concentrations of antibodies against CD3-AF700 (BD Biosciences, clone SP34-2), CD14-APC-H7 (BD Biosciences, clone MφP9), and CD45-V500 (BD Biosciences, clone HI30) (Table 1), washed twice in cold (4 °C) PBS/2 mM ethylenediaminetetraacetic acid (EDTA)/1% BSA, and fixed (1% formaldehyde). Cell association with AF633-labeled particles was analyzed by flow cytometry (LSRFortessa, BD Biosciences), with cell types identified using the gating strategy shown in Figure S6 of the Supporting Information.

**Preparation of Subcutaneous Xenograft Tumors in Mice:** Eight-week-old female Balb/c nu/nu mice were acquired from the Animal Resource Centre. To establish tumors for in vivo targeting experiments,

**Table 1.** Fluorescent antibodies used to phenotype human blood cells.

Antigen	Clone	Fluorophore	Supplier
CD3	SP34-2	AF700	BD Biosciences
CD5	UCHT2	APC	BioLegend
CD14	M $\phi$ P9	APC-H7	BD Biosciences
CD19	H1B19	BV650	BD Biosciences
CD45	HI30	V500	BD Biosciences
CD56	B159	PE	BD Biosciences
CD66b	G10F5	BV421	BD Biosciences
c-Myc	Polyclonal	FITC	Abcam

immunocompromised mice were anesthetized using 2% isoflurane and injected in the left mammary fat pad with  $3 \times 10^6$  MDA-MB-468 cells, each in 80  $\mu$ L serum-free medium using a 27 G needle. Tumors were allowed to grow for 12 days before imaging experiments, at which time all mice had palpable tumors of  $\approx$ 5 mm in diameter.

All animal experiments were approved by The University of Queensland's Animal Ethics Committee (AEC530/15) and conformed to the guidelines of the Australian Code of Practice for the Care and use of Animals for Scientific Purposes.

**Radiolabeling of PEG-110 Particles:**  $^{64}\text{CuCl}_2$  (300  $\mu$ L, 500 MBq) was diluted with 0.1 M ammonium acetate buffer (300  $\mu$ L, pH 5.5). From this stock solution, 50 MBq (40  $\mu$ L) was aliquoted and added to the PEG particles (1 mL, 0.9 mg mL $^{-1}$  in 0.1 M ammonium acetate buffer) and stirred for 1 h at 25  $^{\circ}$ C. Free  $^{64}\text{Cu}$  was removed from the polymers by passing the solution through Zeba Spin Desalting Columns (40 kDa MWCO, 0.5 mL), buffer exchanging into PBS. To assess sample purity, a small aliquot (5  $\mu$ L) was reacted with a large excess of EDTA (1000 molar excess) for 15 min. The solutions were then analyzed with iTLC (mobile phase 50% ethanol in water). The plates were dried and imaged using the In-Vivo MS FX PRO optical imaging system. Radioisotopic images were collected using a phosphor screen and an acquisition time of 60 s (4  $\times$  4 binning, 2.50 f-stop, 190 mm field of view (FOV)). These images were coregistered with a reflectance image (430  $\pm$  10 nm excitation, 1 s exposure, 57 f-stop, 190 mm FOV). Radioisotopic images were false colored and overlaid onto the corresponding reflectance image. The radiolabeled PEG particle bound to  $^{64}\text{Cu}$  had a retention value ( $R_f$ ) of 0 and the  $^{64}\text{Cu}$ -EDTA had an  $R_f$  of 1. Only samples showing a radiochemical purity of greater than 95% via thin layer chromatography analysis (using the Bruker MI software) were used for BsAb conjugation.

**Targeting of PEG-BsAb Particles for In Vivo Imaging:** Four samples were prepared via mixing anti-PEG/anti-EGFR BsAbs (0, 5, 15, and 20  $\mu$ g) with PEG particles and incubated for 8 h at 4  $^{\circ}$ C. For each sample, 12 MBq of the radiolabeled PEG particles was used (4 MBq prepared per mouse,  $n = 3$ ). The radiolabeled PEG-110 particles with different BsAb functionalization (3.00–4.00 MBq per mouse,  $n = 3$ ) were injected intravenously via tail vein.

**Live Animal Imaging and Postmortem Analysis:** Mice were anesthetized with isoflurane (IsoFlo, Abbott Laboratories) at a dose of 2% in a closed anesthetic induction chamber. Mice were monitored using ocular and pedal reflexes to ensure deep anesthesia. Once the mice were deeply anesthetized, they were placed on an appropriate animal bed, where the anesthetic air mixture (1%) was delivered to the nose and mouth through a nose cone. Physiological monitoring (respiratory using a sensor probe) was performed using an animal monitoring system (the BioVet system, m2m Imaging, Australia).

The injection syringe was filled with the radioisotope solution ( $\approx$ 150  $\mu$ L), and the activity in the syringe was measured using a dose calibrator (Capintec CRC-25) with a calibration factor of 35. The residual activity in the syringe after the tail vein injection was measured using the same dose calibrator, and the total volume injected in each mouse was calculated ( $\approx$ 3.00–4.00 MBq). Calibration of the PET/CT scanner was

performed with an in-house-manufactured phantom containing a dose of  $^{64}\text{Cu}$  solution as a radiation source.

The mice were positioned on the scanner bed, and micro-CT scans were acquired for anatomical coregistration. The CT images of the mice were acquired using an X-ray source with the voltage set to 80 kV and the current set to 500  $\mu$ A. The scans were performed using 360 $^{\circ}$  rotation with 120 rotation steps and a low magnification and a binning factor of four. The exposure time was 230 ms with an effective pixel size of 106  $\mu$ m. The total CT scanning process took  $\approx$ 15 min. Following CT imaging, PET scans were acquired at 24 h postinjection of the radiotracer, using 30–60 min static acquisitions.

At 48 h postinjection, mice were sacrificed via cervical dislocation while anesthetized, and their organs collected postmortem into preweighed vials. Each tube was weighed to determine the weight of each organ, and the activity in each organ was measured independently by a WIZARD 2480 Automatic Gamma Counter (WIZARD $^2$ , Perkin Elmer) with a fixed counting window of 15–2000 keV and a detector efficiency of 89%. The activity in the heart, lung, kidney, liver, spleen, and tumor was measured for 60 s as counts per minute.

**Data Analysis:** The CT images were reconstructed using Feldkamp reconstruction software (Siemens). The PET images were reconstructed using an ordered subset expectation maximization (OSEM2D) algorithm and analyzed using the Inveon Research Workplace software (IRW 4.1, Siemens), which allows fusion of CT and PET images and definition of regions of interests (ROIs). CT and PET datasets of each individual animal were aligned using IRW software (Siemens) to ensure good overlap of the organs of interest. 3D ROIs were placed within the whole body, as well as all the organs of interest, such as heart, kidney, lungs, bladder, liver, spleen, intestines, and tumor, using morphologic CT information to delineate organs. Activity per voxel was converted into nanoCurie per cubic centimeter (nCi/cc) using a conversion factor obtained by scanning a cylindrical phantom filled with a known activity of  $^{64}\text{Cu}$  to account for PET scanner efficiency. Activity concentrations were then expressed as percentage of the decay-corrected injected activity per cubic centimeter of tissue that can be approximated as %ID g $^{-1}$ . For validation, the %ID g $^{-1}$  for each organ was also directly calculated from the gamma counter measurements, decay-corrected injected dose, and mass of the organ weighed immediately after dissection. All data were plotted using GraphPad Prism 6.

**Characterization Methods:** The MS templates were imaged by TEM on an FEI Tecnai G2 Spirit microscope, operating at 120 kV. The particle suspension in water was dropped on a carbon film-coated copper grid (ProSciTech, Australia) and air-dried before TEM imaging. Fluorescence images of the PEG particles templated from 1000 and 110 nm MS particles were acquired by an Olympus IX71 inverted fluorescence microscopy equipped with a DIC slider and a DeltaVision OMX super-resolution structured illumination microscope (Applied Precision). CLSM images of the PEG-1000-EGFR particles were obtained on a Nikon A1R confocal microscope with a 100 $\times$  oil immersion objective with a standard FITC/TRITC/CY5 filter sets.

**Statistical Analysis:** Data are expressed as means  $\pm$  standard deviations based on triplicate experiments. Statistical analyses were carried out using the GraphPad software Prism (Version 6.0) by one-way ANOVA with Tukey's multiple comparisons test for Figure 2a,b and two-way ANOVA with Tukey's multiple comparisons test for Figures 2c,d, 3a,b, 6a, and 7. In all cases, significance was defined as  $p \leq 0.05$ .

## Supporting Information

Supporting Information is available from the Wiley Online Library or from the author.

## Acknowledgements

J.C., Y.J., Z.H.H., and J.J.G. contributed equally to this work. This work was conducted and funded by the Australian Research Council (ARC)

Centre of Excellence in Convergent Bio-Nano Science and Technology (Project No. CE140100036). This work was performed in part at the Materials Characterization and Fabrication Platform (MCFP) at The University of Melbourne, the Victorian Node of the Australian National Fabrication Facility (ANFF), and the National Imaging Facility at the Centre for Advanced Imaging (The University of Queensland). F.C. acknowledges the award of a National Health and Medical Research Council (NHMRC) Senior Principal Research Fellowship (APP1135806) and K.J.T. acknowledges the award of an NHMRC Career Development Fellowship (APP1148582). J.C. acknowledges the Thousand Talents Plan Program of China and the National Natural Science Foundation of China (No. 21603120 and No. 21872085). The authors acknowledge scientific discussion and technical assistance from Dr. Karine Mardon (The University of Queensland) and Prof. Christoph E. Hagemeyer (Monash University). The authors thank Dr. Julie McAuley for kindly providing the CHO-K1 cells, Craig A. Bell for his synthetic modifications to the BsAbs, and Hannah Kelly and Thakshila Amarasena for their assistance with the whole blood assay.

## Conflict of Interest

The authors declare no conflict of interest.

## Keywords

biodistribution, bispecific antibodies, cell targeting, mesoporous silica particles, PEG particles

Received: December 16, 2018

Revised: February 13, 2019

Published online:

- [1] a) J. Liu, M. Li, Z. Luo, L. Dai, X. Guo, K. Cai, *Nano Today* **2017**, *15*, 56; b) K. M. Tsoi, S. A. MacParland, X.-Z. Ma, V. N. Spetzler, J. Echeverri, B. Ouyang, S. M. Fadel, E. A. Sykes, N. Goldaracena, J. M. Kathis, *Nat. Mater.* **2016**, *15*, 1212; c) S. Wilhelm, A. J. Tavares, Q. Dai, S. Ohta, J. Audet, H. F. Dvorak, W. C. Chan, *Nat. Rev. Mater.* **2016**, *1*, 16014; d) M. Yu, J. Zheng, *ACS Nano* **2015**, *9*, 6655.
- [2] a) E. Blanco, H. Shen, M. Ferrari, *Nat. Biotechnol.* **2015**, *33*, 941; b) Z. Cao, S. Jiang, *Nano Today* **2012**, *7*, 404; c) S. Lowe, N. M. O'Brien-Simpson, L. A. Connal, *Polym. Chem.* **2015**, *6*, 198; d) E. M. Pelegri-O'Day, E. W. Lin, H. D. Maynard, *J. Am. Chem. Soc.* **2014**, *136*, 14323.
- [3] J. S. Suk, Q. Xu, N. Kim, J. Hanes, L. M. Ensign, *Adv. Drug Delivery Rev.* **2016**, *99*, 28.
- [4] a) X. J. Du, J. L. Wang, W. W. Liu, J. X. Yang, C. Y. Sun, R. Sun, H. J. Li, S. Shen, Y. L. Luo, X. D. Ye, Y. H. Zhu, X. Z. Yang, J. Wang, *Biomaterials* **2015**, *69*, 1; b) Q. Yang, S. W. Jones, C. L. Parker, W. C. Zamboni, J. E. Bear, S. K. Lai, *Mol. Pharmaceutics* **2014**, *11*, 1250.
- [5] a) J. Cui, R. De Rose, K. Alt, S. Alcantara, B. M. Paterson, K. Liang, M. Hu, J. J. Richardson, Y. Yan, C. M. Jeffery, R. I. Price, K. Peter, C. E. Hagemeyer, P. S. Donnelly, S. J. Kent, F. Caruso, *ACS Nano* **2015**, *9*, 1571; b) J. Cui, M. Björnalm, K. Liang, C. Xu, J. P. Best, X. Zhang, F. Caruso, *Adv. Mater.* **2014**, *26*, 7295; c) D. Song, J. Cui, H. Sun, T. H. Nguyen, S. Alcantara, R. De Rose, S. J. Kent, C. J. H. Porter, F. Caruso, *ACS Appl. Mater. Interfaces* **2017**, *9*, 33683.
- [6] a) B. Yu, H. Wei, Q. He, C. A. Ferreira, C. J. Kutyreff, D. Ni, Z. T. Rosenkrans, L. Cheng, F. Yu, J. W. Engle, X. Lan, W. Cai, *Angew. Chem.* **2018**, *130*, 224; *Angew. Chem. Int. Ed.* **2018**, *57*, 218;
- b) Y. Dai, S. Cheng, Z. Wang, R. Zhang, Z. Yang, J. Wang, B. C. Yung, Z. Wang, O. Jacobson, C. Xu, Q. Ni, G. Yu, Z. Zhou, X. Chen, *ACS Nano* **2018**, *12*, 455; c) Y. Dai, J. Guo, T. Y. Wang, Y. Ju, A. J. Mitchell, T. Bonnard, J. Cui, J. J. Richardson, C. E. Hagemeyer, K. Alt, F. Caruso, *Adv. Healthcare Mater.* **2017**, *6*, 1700467; d) Y. Dai, Z. Yang, S. Cheng, Z. Wang, R. Zhang, G. Zhu, Z. Wang, B. C. Yung, R. Tian, O. Jacobson, C. Xu, Q. Ni, J. Song, X. Sun, G. Niu, X. Chen, *Adv. Mater.* **2018**, *30*, 1704877.
- [7] D. J. Irvine, M. C. Hanson, K. Rakhra, T. Tokatlian, *Chem. Rev.* **2015**, *115*, 11109.
- [8] M. Björnalm, K. J. Thurecht, M. Michael, A. M. Scott, F. Caruso, *ACS Nano* **2017**, *11*, 9594.
- [9] a) R. V. J. Chari, *Acc. Chem. Res.* **2008**, *41*, 98; b) S. T. Gunawan, K. Kempe, T. Bonnard, J. Cui, K. Alt, L. S. Law, X. Wang, E. Westein, G. K. Such, K. Peter, C. E. Hagemeyer, F. Caruso, *Adv. Mater.* **2015**, *27*, 5153; c) Q. Dai, N. Bertleff-Zieschang, J. A. Braunger, M. Björnalm, C. Cortez-Jugo, F. Caruso, *Adv. Healthcare Mater.* **2018**, *7*, 1700575.
- [10] a) A. J. Sivaram, A. Wardiana, C. B. Howard, S. M. Mahler, K. J. Thurecht, *Adv. Healthcare Mater.* **2018**, *7*, 1700607; b) D. A. Richards, A. Maruani, V. Chudasama, *Chem. Sci.* **2017**, *8*, 63.
- [11] a) D. Chelius, P. Ruf, P. Gruber, M. Plösch, R. Liedtke, E. Gansberger, J. Hess, M. Wasiliu, H. Lindhofer, *mAbs* **2010**, *2*, 309; b) C. Sheridan, *Nat. Biotechnol.* **2015**, *33*, 219; c) U. Brinkmann, R. E. Kontermann, *mAbs* **2017**, *9*, 182.
- [12] a) L. J. Raftery, Y. S. Grewal, C. B. Howard, M. L. Jones, M. J. A. Shiddiky, L. G. Carrascosa, K. J. Thurecht, S. M. Mahler, M. Trau, *Chem. Commun.* **2016**, *52*, 5730; b) C. B. Howard, N. Fletcher, Z. H. Houston, A. V. Fuchs, N. R. Boase, J. D. Simpson, L. J. Raftery, T. Ruder, M. L. Jones, C. J. de Bakker, S. M. Mahler, K. J. Thurecht, *Adv. Healthcare Mater.* **2016**, *5*, 2055.
- [13] Y. Ju, J. Cui, H. Sun, M. Mullner, Y. Dai, J. Guo, N. Bertleff-Zieschang, T. Suma, J. J. Richardson, F. Caruso, *Biomacromolecules* **2016**, *17*, 2268.
- [14] a) H. S. S. Qhattal, T. Hye, A. Alali, X. Liu, *ACS Nano* **2014**, *8*, 5423; b) F. Gu, L. Zhang, B. A. Teply, N. Mann, A. Wang, A. F. Radovic-Moreno, R. Langer, O. C. Farokhzad, *Proc. Natl. Acad. Sci. USA* **2008**, *105*, 2586.
- [15] K. Taylor, C. B. Howard, M. L. Jones, I. Sediarou, J. MacDiarmid, H. Brahmabhatt, T. P. Munro, S. M. Mahler, *mAbs* **2015**, *7*, 53.
- [16] Q. Sun, Z. Zhou, N. Qiu, Y. Shen, *Adv. Mater.* **2017**, *29*, 1606628.
- [17] A. P. R. Johnston, M. M. J. Kamphuis, G. K. Such, A. M. Scott, E. C. Nice, J. K. Heath, F. Caruso, *ACS Nano* **2012**, *6*, 6667.
- [18] N. Kotagiri, Z. Li, X. Xu, S. Mondal, A. Nehorai, S. Achillefu, *Bioconjugate Chem.* **2014**, *25*, 1272.
- [19] T. L. Cheng, S. R. Roffler, K. H. Chuang, S. J. Lu (Kaohsiung Medical University), *US20120015380A1*, **2011**.
- [20] X. D. Yang, X. C. Jia, J. R. Corvalan, P. Wang, C. G. Davis, *Crit. Rev. Oncol./Hematol.* **2001**, *38*, 17.
- [21] S. Puttick, B. W. Stringer, B. W. Day, Z. C. Bruce, K. S. Ensbe, K. Mardon, G. J. Cowin, K. J. Thurecht, A. K. Whittaker, M. Fay, *Mol. Imaging* **2015**, *14*, 385.
- [22] J. G. Wang, H.-J. Zhou, P.-C. Sun, D.-T. Ding, T.-H. Chen, *Chem. Mater.* **2010**, *22*, 3829.
- [23] K. Zhang, L. L. Xu, J. G. Jiang, N. Calin, K. F. Lam, S. J. Zhang, H. H. Wu, G. D. Wu, B. Albela, L. Bonneviot, P. Wu, *J. Am. Chem. Soc.* **2013**, *135*, 2427.
- [24] M. Björnalm, J. Cui, N. Bertleff-Zieschang, D. Song, M. Faria, M. A. Rahim, F. Caruso, *Chem. Mater.* **2017**, *29*, 289.
- [25] H.-Y. Tung, Y.-C. Su, B.-M. Chen, P.-A. Burnouf, W.-C. Huang, K.-H. Chuang, Y.-T. Yan, T.-L. Cheng, S. R. Roffler, *Mol. Cancer Ther.* **2015**, *14*, 1317.